Structural variation along the Devil's Mountain fault zone, northwestern Washington

Nathan Hayward, Mladen R. Nedimović, Matthew Cleary, and Andrew J. Calvert

Abstract: The eastern Juan de Fuca Strait is subject to long-term, north–south-oriented shortening. The observed deformation is interpreted to result from the northward motion of the Oregon block, which is being driven north by oblique subduction of the oceanic Juan de Fuca plate. Seismic data, acquired during the Seismic Hazards Investigation in Puget Sound survey are used, with coincident first-arrival tomographic velocities, to interpret structural variation along the Devil's Mountain fault zone in the eastern Juan de Fuca Strait. The Primary fault of the Devil's Mountain fault zone developed at the northern boundary of the Everett basin, during north–south-oriented Tertiary compression. Interpretation of seismic reflection data suggests that, based on their similar geometry including the large magnitude of pre-Tertiary basement offset, the Primary fault of the Devil's Mountain fault west of ~122.95°W and the Utsalady Point fault represent the main fault of the Tertiary Devil's Mountain fault zone. The Tertiary Primary fault west of ~122.95°W was probably kinematically linked to faults to the east (Utsalady Point, Devil's Mountain, and another to the south), by an oblique north–northeast-trending transfer zone or ramp. Left-lateral transpression controlled the Quaternary evolution of the Devil's Mountain fault zone. Quaternary Primary fault offsets are smaller to the east of ~122.95°W, suggesting that stress here was in part accommodated by the prevalent oblique compressional structures to the north. Holocene deformation has focussed on the Devil's Mountain, Utsalady Point, and Strawberry Point faults to the east of ~122.8° but has not affected the Utsalady Point fault to the west of ~122.8°W.

Résumé : L'est du détroit de Juan de Fuca est sujet, à long terme, à un rétrécissement orienté nord–sud. On croit que la déformation observée résulte du mouvement vers le nord du bloc Oregon, lequel est poussé vers le nord par une subduction oblique de la plaque océanique Juan de Fuca. Des données sismiques acquises au cours de relevé SHIPS (« Seismic Hazards Investigation in Puget Sound ») sont utilisées, de concert avec l'arrivée des premières vitesses tomographiques, pour interpréter la variation structurale le long de la zone de failles de Devil's Mountain dans l'est du détroit de Juan de Fuca. La faille Primary de la zone de failles de Devil's Mountain s'est développée à la limite nord du bassin Everett durant la compression nord–sud au cours du Tertiaire. Selon l'interprétation des données de sismique réflexion et en se basant sur leur géométrie similaire, incluant le grand décalage du socle avant le Tertiaire, la faille Primary de la zone de failles de Devil's Mountain, à l'ouest de ~122,95°W, et la faille d'Utsalady Point représentent la faille principale de la zone de failles de Devil's Mountain (Tertiaire). La faille Primary (Tertiaire) à l'ouest de ~122,95°W était probablement reliée de manière cinématique aux failles à l'est (Utsalady Point, Devil's Mountain et une autre plus au sud) par une zone ou une rampe de transfert oblique à tendance NNE. Une transpression latérale senestre contrôlait l'évolution de la zone de failles de Devil's Mountain au Quaternaire. Les décalages de la faille Primary durant le Quaternaire sont plus faibles à l'est de ~122,95°W, suggérant que la contrainte soit ici partiellement englobée par les structures obliques de compression qui prévalaient au nord. La déformation au cours de l'Holocène ciblait les failles de Devil's Mountain, d'Utsalady Point et de Strawberry Point à l'est de ~122,8° mais n'a pas touché la faille d'Utsalady Point à l'ouest de ~122,8°W.

[Traduit par la Rédaction]

Introduction

The eastern Juan de Fuca Strait lies southeast of Vancouver Island (Fig. 1) on the southwestern margin of Canada and the northwestern United States. The strait is underlain by a complex system of faults, including the Devil's Mountain fault and Southern Whidbey Island fault (Gower et al. 1985), whose structure and tectonic evolution are not fully understood. Crustal seismicity, with magnitudes of up to ~4 (Weaver and Smith 1983), have been recorded for the east-

Received 31 March 2005. Accepted 10 January 2006. Published on the NRC Research Press Web site at http://cjes.nrc.ca on 4 May 2006.

Paper handled by Associate Editor K. Ansdell.

N. Hayward, M. Cleary, and A.J. Calvert.[1] Simon Fraser University, Department of Earth Sciences, 8888 University Drive, Burnaby, BC V5A 1S6, Canada.
M.R. Nedimović. Department of Marine Geology and Geophysics, Lamont-Doherty Earth Observatory, Columbia University, 61 Route 9W, P.O. Box 1000, Palisades, NY 10964-8000, USA.

[1]Corresponding author (e-mail: acalvert@sfu.ca).

 doi:10.1139/E06-002

Fig. 1. Tectonic setting. Fault Zones: DMFZ, Devil's Mountain; SWFZ, Southern Whidbey Island; SJF, San Juan; SMF, Survey Mountain; LRF, Leech River; OB, Oregon Block, with half arrows (schematically from Wells et al. 1998) representing the rotation. Area in grey dashed box to the lower right shows the location of study area (shown in Fig. 2).

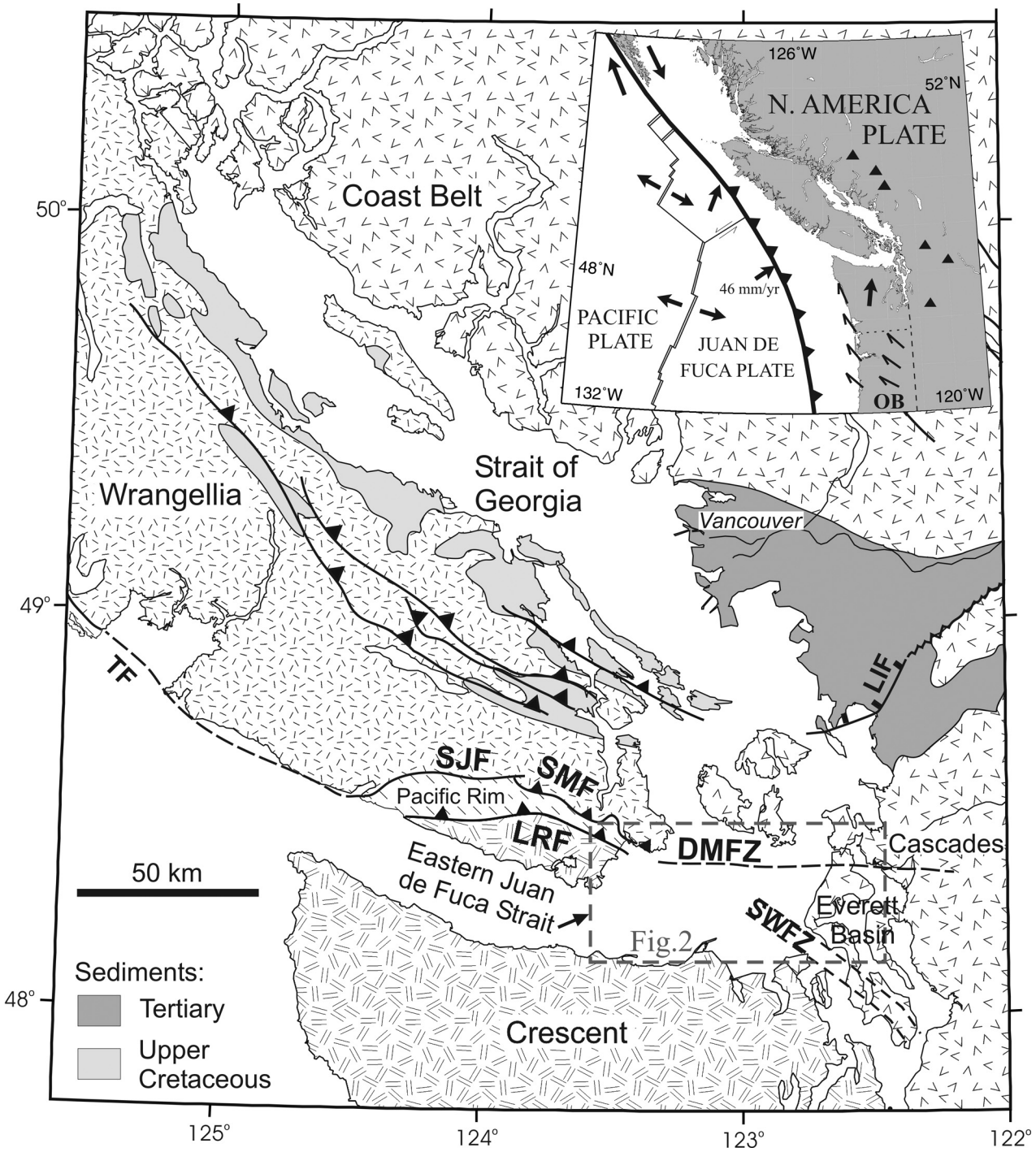

ern Juan de Fuca Strait region, and large prehistoric crustal earthquakes have been inferred (Gower et al. 1985; Atwater and Moore 1992). Major fault zones, such as the Devil's Mountain and Southern Whidbey Island, are probably active today and may represent the location of potentially hazardous crustal earthquakes.

The Devil's Mountain fault became active in the Late Eocene, following a complex tectonic evolution that prior to this time was associated with right-lateral strike-slip motion on the NNE-trending Coast Range Boundary fault and Southern Whidbey Island fault (Johnson et al. 1996). The exotic terranes, including the Crescent and Pacific Rim terranes, which now form the eastern Juan de Fuca Strait's structurally complex and lithologically variable basement, had accreted by the Early–Middle Eocene (~42 Ma) (Hyndman et al. 1990). Accretion coincided with the initia-

tion of oblique oceanic subduction to the west (Hyndman et al. 1990) and resulted in a kinematic reorganization (Johnson et al. 1996) that included the onset of north–south-directed shortening. Compression, with a possibly right-lateral component (Tabor 1994), commenced on the Devil's Mountain fault in the Late Eocene (Johnson et al. 1996), accompanied by decreasing activity along the Southern Whidbey Island fault. The Devil's Mountain fault formed the northern boundary of the Tertiary Everett basin (Johnson et al. 1996), one of several tectonically isolated basins of great stratigraphic diversity on the western Washington margin (Johnson 1985). Quaternary en-echelon faults and folds with a northwest strike, in a zone of over a width of 10 km along the east-trending Devil's Mountain fault strongly suggest that the Devil's Mountain fault during this later time was a left-lateral transpressional fault (Johnson et al. 2000, 2001).

Tectonic forces, resulting from subduction, drive current deformation in the Devil's Mountain fault zone. The Juan de Fuca oceanic plate is currently subducting northeastwards beneath the Cascadia margin (Fig. 1, inset) at ~ 46 mm a^{-1}. The majority of related strain in the overlying North American plate, measured geodetically on land, is oblique (at a high angle) to the plate boundary because of the locking of the interplate interface (e.g., Dragert et al. 1994). An integral part of the kinematics of the Cascadia subduction zone is the northward, margin-parallel migration of the Oregon block (e.g., Wells et al. 1998; McCaffrey et al. 2000) (Fig. 1). Earthquake focal mechanisms for events within the northwestern Washington – southwestern British Columbia region (e.g., Lewis et al. 2003; Wells et al. 1998) show that it is a region of distributed strain. In the Devil's Mountain fault zone, the current shortening has a generally northward direction (Lewis et al. 2003). Global positioning system (GPS) measurements indicate a north–south shortening rate of 3 ± 1 mm a^{-1} (Hyndman et al. 2003), similar to the 2–3 mm a^{-1} rate derived from crustal earthquake statistics for the Puget–Georgia basin (Hyndman et al. 2003). The long-term shortening rate, following the removal of the subduction-related interseismic loading of the margin and signal owing to the postglacial rebound from the total GPS velocity field, is ~5–6 mm a^{-1} (Mazzotti et al. 2002).

Previous investigations in the eastern Juan de Fuca Strait (e.g., Mosher and Johnson 2000; Johnson et al. 2001) have revealed that complex faulting and folding affected Tertiary to Recent sedimentary rocks. These sedimentary rocks lie unconformably upon pre-Tertiary and Eocene basement rocks. Pleistocene glaciers (Booth 1994) eroded near-surface rocks removing evidence of surface faulting. Deposition of a blanket of glacial sediments masked shallow pre-Pleistocene structures (Hewitt and Mosher 2001). By the early Holocene, sea level may have been 60 m lower than at present (Mosher and Hewitt 2004). A lower sea level would have exposed bathymetric highs to further erosion, removing evidence of recent faulting and deformation. Deposition of the eroded sediments further complicates the interpretation of recent tectonic activity and the assessment of the risk posed by various faults in the region.

In this study, we use seismic data from the Seismic Hazards Investigation in Puget Sound (SHIPS) survey (Fisher et al. 1999) to create coincident tomographic velocity models and reflection profiles. In combination, these elucidate the shallow structure of the eastern Juan de Fuca Strait and provide new information on the along-strike variation of the Devil's Mountain fault and its related structures. These observations lead to new interpretations of the structure of the Devil's Mountain fault zone.

Tomographic modelling and reflection seismic processing

Multichannel seismic data from the SHIPS survey (Fig. 2) (Fisher et al. 1999) were acquired using a 2.5 km long, 96-channel streamer with receiver group interval of 25 m and a 2575 m far offset. The acoustic source was a 13-airgun array (79.3 L) fired every 22 s. The recording time was 16 s with a 4 ms interval. Nominal common midpoint (CMP) fold is 24. First-pass reflection processing was conducted by the US Geological Survey (Fisher et al. 1999). However, because the data were processed to enhance features to 16 s two-way travel time, they lack clear imaging of the shallow reflections.

New seismic reflection processing

Straight-line sections of seismic reflection data from the SHIPS lines JDF-1, JDF-2, JDF-3, JDF-4, JDF-5, JDF-6, PS-2, and SG-1 (Fig. 2) were reprocessed at the Geological Survey of Canada. Extracting reflection structure from data collected in a shallow waterway with a hard water-bottom, such as in the eastern Juan de Fuca Strait, is challenging. Reflections are masked by refracted waves, multiples, side-scattered energy, ship noise, and other high-amplitude broadband cultural noise. Imaging was further hindered by a dynamic reflection traveltime anomaly introduced by greater streamer depth at far offsets and possibly by the lack of information on streamer feathering (Nedimović et al. 2003).

To extract maximum structural information from the data and to be able to accurately tie the images to the subsurface structures, the geometry was assigned using the variable shot spacing. This has significantly improved the image quality in the near surface. The true shot spacing varied between ~30 and 70 m, compared with an originally assumed constant shot separation of 50 m. For example, the average shot spacing on profile JDF-6 is 41.46 m, resulting in a line that is ~6 km shorter than one created when assuming a constant shot separation of 50 m. Compressing the length of such a line to its true length by linear means would not account for along-line variations in shot spacing and would result in the erroneous location of geological features. An amplitude correction was applied for geometrical spreading, and the data were deconvolved with a minimum-phase, spiking deconvolution operator. A surface-consistent amplitude correction was applied, and the data filtered with a 57–59 – 61–63 Hz notch and 1–6 – 100–120 Hz bandpass filter. Software was written to build shot and receiver co-ordinates into the trace headers. Crooked line geometry was then assigned based on a slalom line through the shot/receiver midpoints. These data were used to calculate the number and co-ordinates of CMP bins in each line segment, which were then used to bin the data traces. Velocity analysis and normal moveout were applied prior to slant stacking and rho filtering, which reduce noise and high-frequency signal losses. Profiles JDF-1, JDF-2. JDF-3, PS-2, and SG-1 were also Tau-P filtered in the upper 4 s to suppress multiples.

Fig. 2. Structural map of Johnson et al. (2000) with the locations of Seismic Hazards Investigation in Puget Sound reflection lines shown in light grey. Dark grey lines are the straight-line sections used in seismic reflection reprocessing and tomographic velocity modelling. The approximate boundary between the pre-Tertiary and Crescent basement is shown by a heavy grey dashed line. Profiles shown in this paper in Figs. 3 and 4, are demarcated by A–A′, B–B′, etc. DMF, Devil's Mountain fault; SWFZ, Southern Whidbey Island fault zone; LRF, Leech River fault; TIF, Trial Island fault.

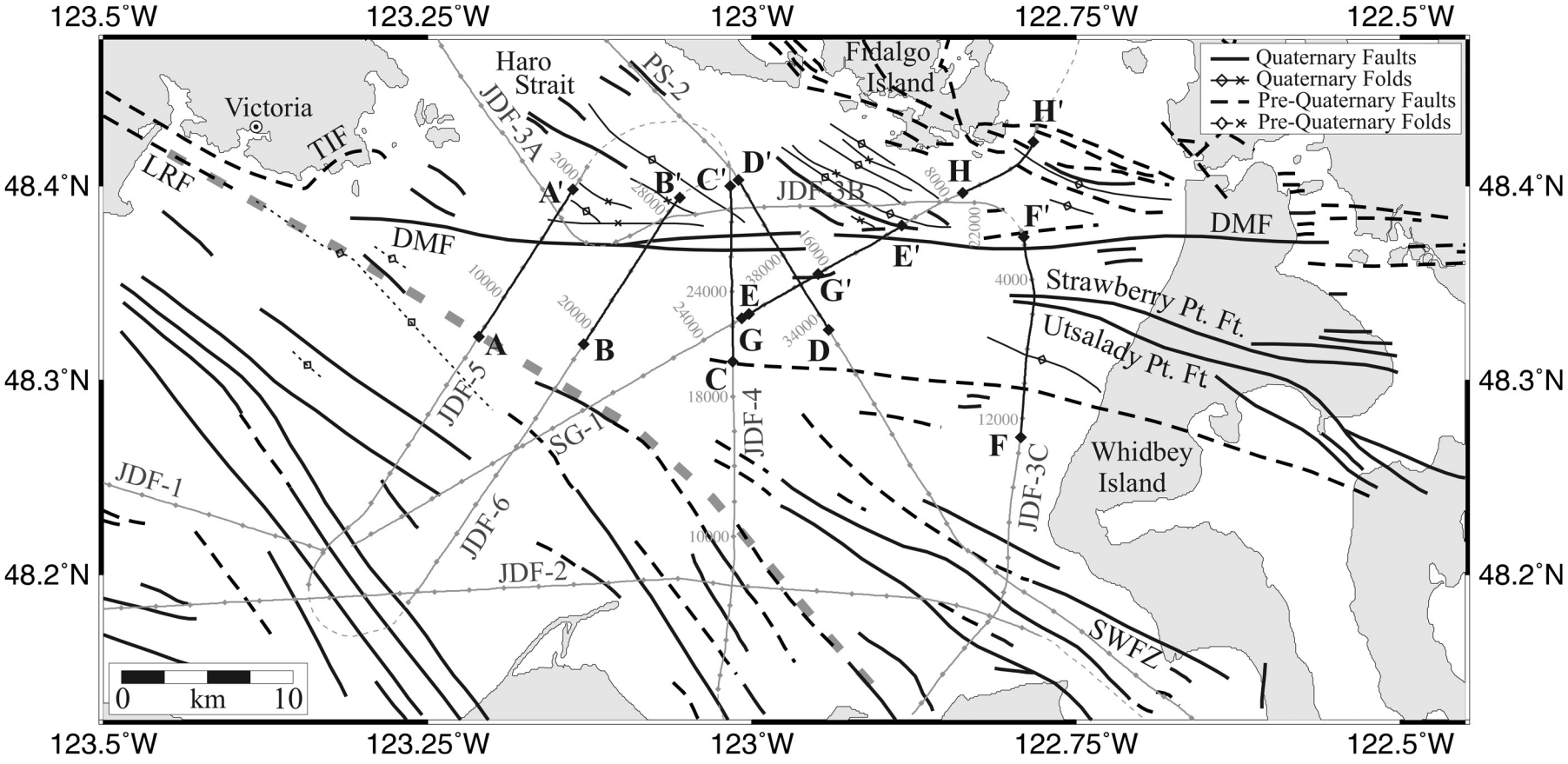

First-arrival tomographic modelling

Velocity models were derived by two-dimensional iterative tomographic inversion of first arrivals (the direct wave and sub-sea-floor refraction) using the true receiver/shot geometry (Calvert et al. 2003) for all straight-line sections of the seismic profiles. A finite-difference solution to the eikonal equation provided first arrival times to all points of a subsurface velocity grid. Raypaths, from each receiver to the source, were generated following the steepest descent direction through the computed travel-times. For each iteration, a perturbation in the velocity model was calculated from the difference between the calculated and observed first arrival travel times (Aldridge and Oldenburg 1993). The velocity of the water layer was set to 1488 ms^{-1} and the sea-floor depth, which was estimated from the arrival of the near-offset reflection channel, was fixed in the inversion. A one-dimensional, three-layer, sub-sea-floor starting model was constructed from a few trial inversions and used as a starting point for 15 iterations with a velocity grid spacing of 25 m.

With far offsets of ~2600 m and a high density of subsurface raypaths, a high-resolution estimate of *P*-wave velocity structure is calculated for depths as large as 500–1200 m. In the eastern Juan de Fuca Strait, this depth corresponds, in all but the deepest regions of the basin, to a depth greater than the base of the uppermost Pliocene; a prominent high-amplitude, unconformity-related reflector (Johnson et al. 2001). Ray density images were used to assess the reliability of the velocity models.

Interpretation of seismic reflection profiles and velocity models

Interpretations of seismic reflection profiles in combination with tomographic velocity models provide new information on structures associated with the Devil's Mountain fault zone (Fig. 2). The location and style of faulting has been enhanced in many areas, and several previously unknown features have been identified.

To facilitate direct comparison of velocity models with seismic reflection profiles, velocity models in depth were converted to two-way travel time (assuming vertically incident rays) and then combined with coincident reflection images. The velocity models show an overall strong correlation to the reflection images, with variation in the magnitudes and gradients of velocity that are coincident with structural and stratigraphic changes.

On a regional scale, structures in the eastern Juan de Fuca Strait follow fairly well-defined trends, creating a pattern that has been tied to strike-slip faulting mechanisms (Christie-Blick and Biddle 1985). Beneath the eastern Juan de Fuca Strait, the Devil's Mountain fault is a discrete east-trending left-lateral transpressive fault adjacent to numerous obliquely oriented faults and folds (Fig. 2) that form a deformational zone with a width greater than 10 km.

The Devil's Mountain fault zone

Setting of the Devil's Mountain fault

The Devil's Mountain fault is a major structure in the eastern Juan de Fuca Strait. The fault formed in the Late Eocene (Johnson et al. 1996), possibly as part of a passive roof duplex (Oldow 2000), at the northern boundary of the Tertiary Everett basin (Johnson et al. 1996). Shallow pre-Tertiary basement rocks outcrop to the north of the fault, and Oligocene Bulson Creek rocks overly the pre-Tertiary basement (Johnson et al. 1996) that underlies most of the study region to the south of the Devil's Mountain fault. Onshore, at the southeast corner of Vancouver Island, the Leech River fault, which is mapped as a northeast-dipping thrust, divides the pre-Tertiary Pacific Rim terrane from the Eocene Crescent terrane (MacLeod et al. 1977; Clowes et al. 1987; Brocher et al. 2001). Offshore, this boundary (Fig. 2) is associated with high-amplitude magnetic anomalies (Johnson et al. 2001), and faulting and pre-Quaternary folding that trend southeast from near Victoria. Onshore, the northern contact of the Pacific Rim terrane with the Wrangellia terrane is marked by the San Juan and Survey Mountain faults (Muller 1983; Rusmore and Cowan 1985). In the southeast corner of Vancouver Island, the Survey Mountain fault is interpreted to be a northeast-dipping thrust (Rusmore and Cowan 1985). Although the Devil's Mountain fault zone has not been traced onto Vancouver Island, it projects into the region just south of Victoria where the northeast-dipping Leech River and Survey Mountain faults are less than 2 km apart and continue offshore.

The Devil's Mountain fault has been mapped offshore, primarily using high-resolution single-channel and industry multichannel seismic reflection profiles (Johnson et al. 2000). The fault follows an easterly trend from Vancouver Island across the northeastern Juan de Fuca Strait (Fig. 2). The Devil's Mountain fault crosses northern Whidbey Island, where it is interpreted to be steeply north dipping (Oldow 2000), and the Skagit River delta before it turns to the southeast (Oldow 2000), where it merges with the south–southeast-trending Darrington (Tabor 1994) and Straight Creek (Oldow 2000) faults. Johnson et al. (2001) interpreted the Devil's Mountain fault in the eastern Juan de Fuca Strait to be a northward-dipping (45°–75°) fault. The numerous northwest-striking en-echelon structures, such as those south of the San Juan Island and in Haro Strait (Fig. 2), are strongly suggestive of left-lateral transpression during the Quaternary (Johnson et al. 2001).

New information on the structure and style of the Devil's Mountain fault zone and its along-strike variation are provided by the SHIPS seismic reflection profiles and tomographic velocity models. The identification of primary structures and of key unit boundaries, such as the base of the uppermost Pliocene and top of the pre-Tertiary basement, were in part based on the interpretations of Johnson et al. (2000, 2001).

Along-strike variation of the Devil's Mountain fault zone

The along-strike variation of the Devil's Mountain fault zone reflects a complex tectonic history and varied basement structure of the eastern Juan de Fuca Strait. Our images show that the accommodation of motion has been distributed among different faults within the Devil's Mountain fault zone throughout its history.

To the southeast of Victoria (Fig. 2), the Devil's Mountain fault is associated with a large vertical offset of the pre-Tertiary basement and Tertiary to Quaternary sedimentary rocks, which we will refer to as the "Primary fault" (Fig. 3*a*, A–A′ (JDF-5); Fig. 3*b*, B–B′ (JDF-6)). Pre-Quaternary rocks

Fig. 3. Structural variation along the Devil's Mountain fault zone. (*a–f*) First-arrival tomographic velocity models overlain on seismic reflection profiles. Vertical exaggeration ~3:1. Black and yellow dashed lines indicate faults. Devil's Mountain fault: black and yellow and black and white dashed lines, estimated range of dip; yellow dots, base of the uppermost Pliocene; red diamonds, top of the Pre-Tertiary basement; red arrows, Tertiary Primary fault of the Devil's Mountain fault. See Fig. 2 for locations.

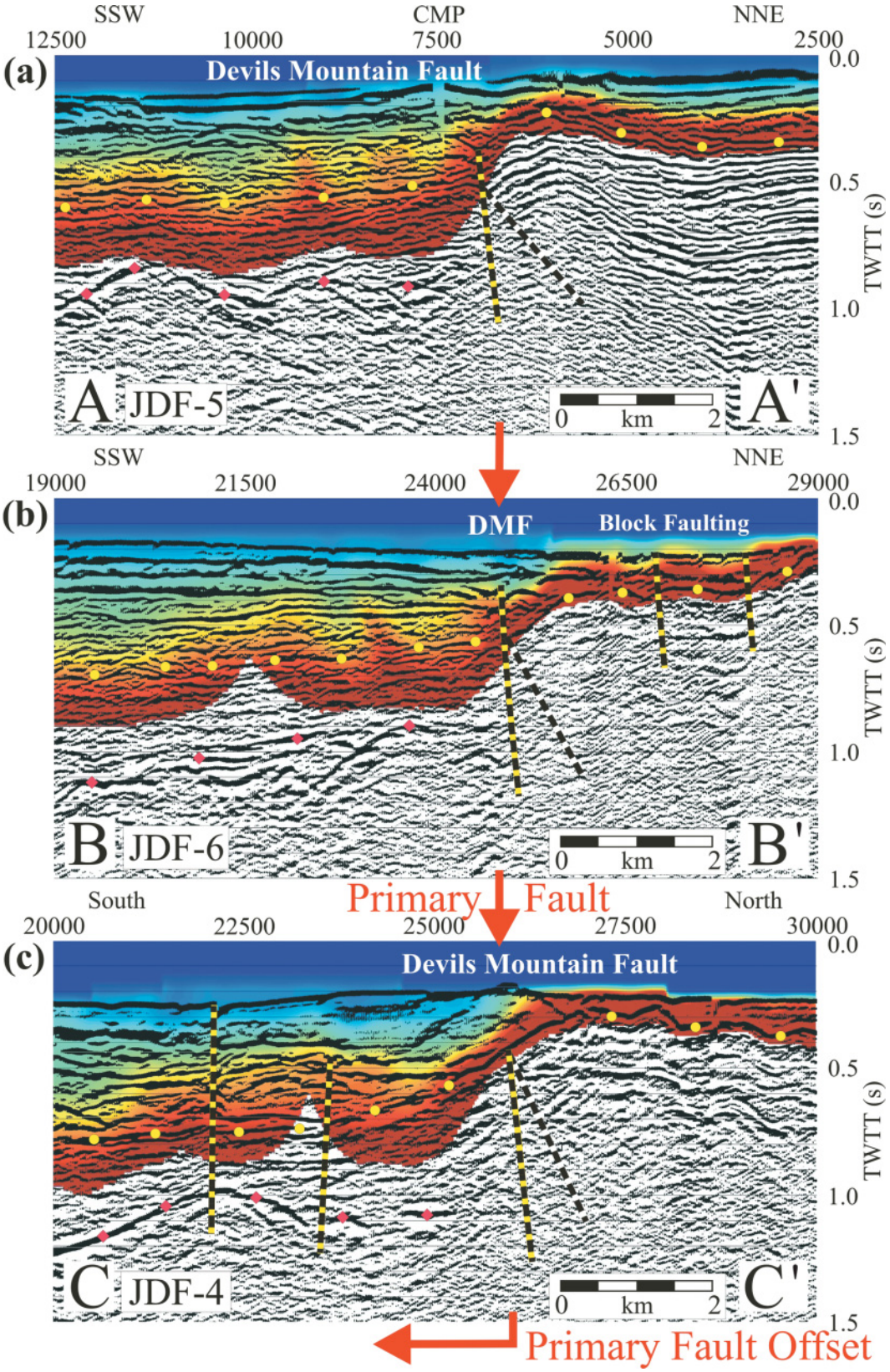

Fig. 3 (*concluded*).

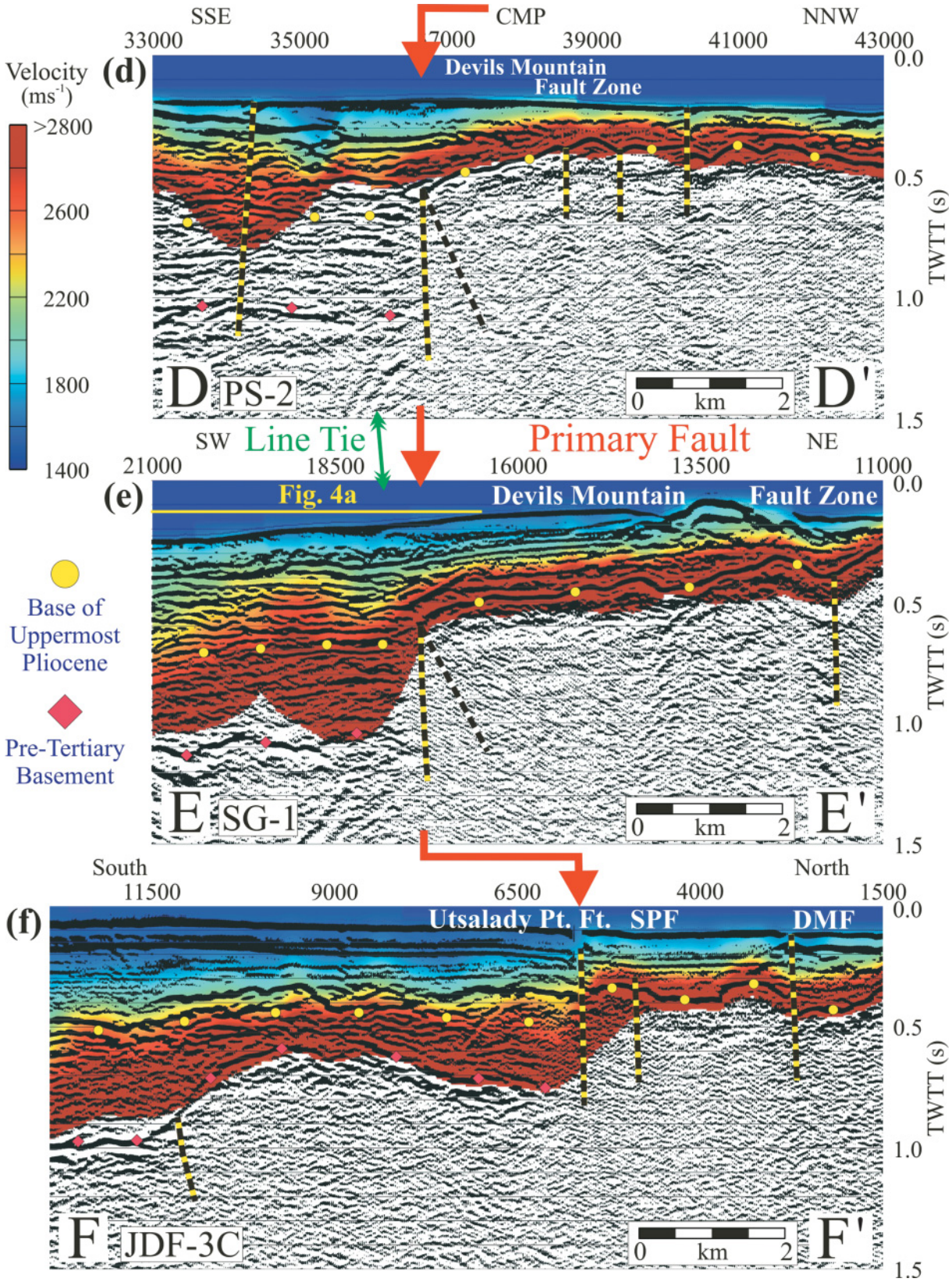

in the hanging wall (north of fault) exhibit anticlinal folding associated with movement on the Devil's Mountain fault. Reflection terminations on either side of the fault zone and north-dipping reflections further north constrain the dip of the fault to be subvertical to north dipping at an angle greater than ~30°. The relative north-up offset is ~0.25 s for the

Fig. 4. (*a*) Section from SG-1 showing faulting to the south of the Devil's Mountain fault. (*b*) Seismic reflection profile from SG-1 showing Quaternary faulting north of the Devil's Mountain fault. Yellow dots, base of the uppermost Pliocene.

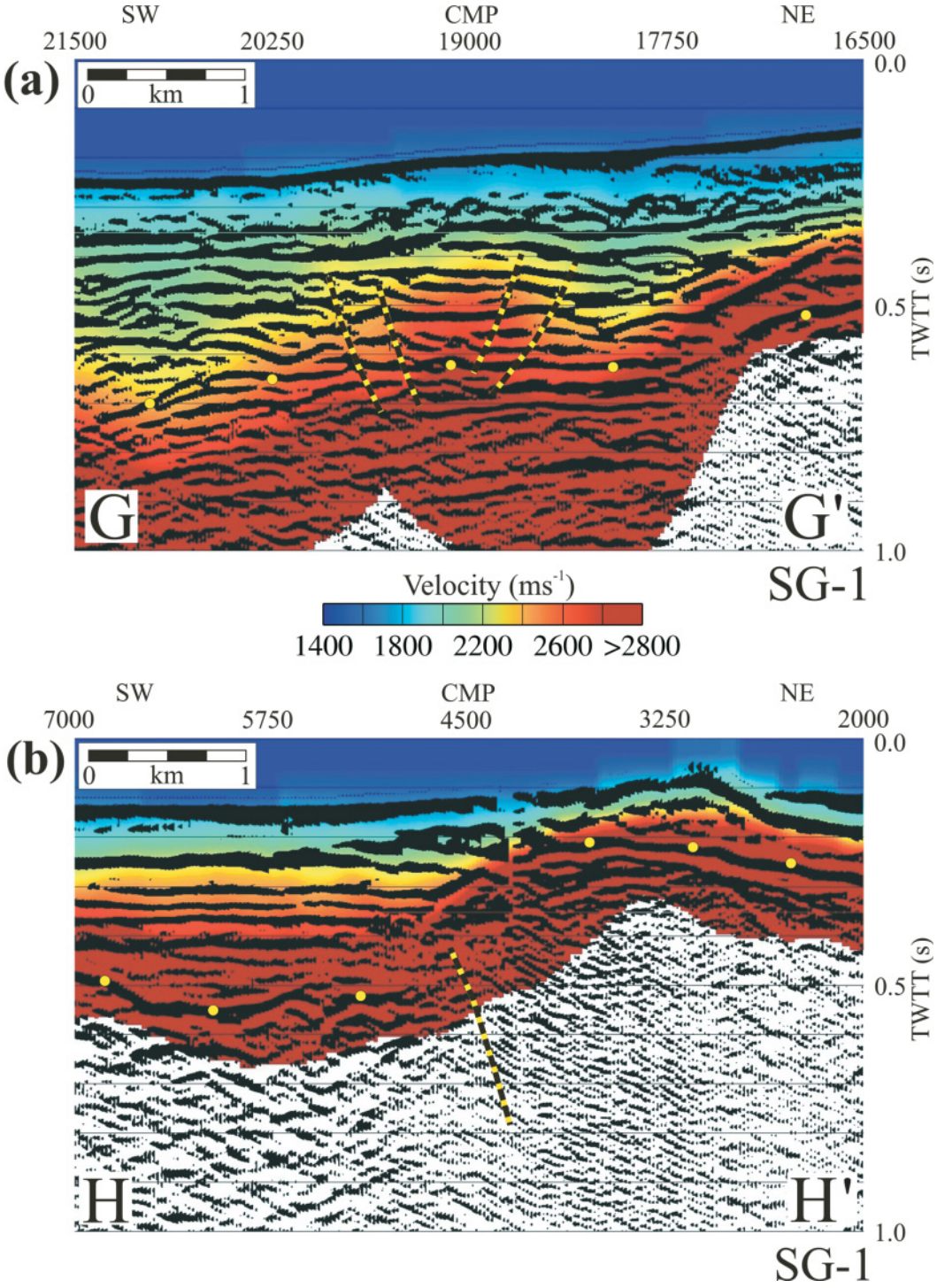

base of the uppermost Pliocene unconformity on both profiles (Fig. 3, yellow dots). This offset coincides with a ~200 m offset in the velocity model. The high-velocity (>5000 ms^{-1}) pre-Tertiary basement is shallow to the north of the Devil's Mountain fault (~0.3 s below sea floor), but the basement at ~0.9–0.95 s is deeper than the base of the velocity model to the south.

Section A–A′ (Fig. 3*a*) shows gentle folding of the uppermost Pliocene, but the deeper parallel reflections north of CMP 5000 are probably multiples. Pleistocene rocks exhibit diffuse deformation away from the Devil's Mountain fault, in contrast to the overlying transparent Holocene sediments, which generally only show deformation in discrete zones associated with more recent active faulting.

Section B–B′ shows high-velocity gradients to the north of the Devil's Mountain fault, which correspond to the shallow

depth (~0.2–0.25 s below sea floor) of the pre-Tertiary basement, probably Wrangellian terrane (Hyndman et al. 1990). The pre-Tertiary basement to the south of the Devil's Mountain fault is slightly deeper than on section A–A′ at ~0.95–1.1 s. Profile JDF-6 images deformed Quaternary rocks north of the Devil's Mountain fault, interpreted by Johnson et al. (2000) to be folded (Fig. 2). However, velocity models show vertical offsets in velocities that cut the shallow sediments. The velocity model shows a rugose topography at the top of the high-velocity basement. We interpret this lateral variation in depth to basement as arising from faulting that disrupts seismic reflections at 0.3 s and divides the pre-Tertiary basement north of the Devil's Mountain fault into three fault-bounded basement blocks (Fig. 3*b*). Changes in reflection character across the Devil's Mountain fault are less marked than on section A–A′, suggesting a broader zone of faulting. The dip of the Devil's Mountain fault is again constrained by truncated reflections to be subvertical to moderately north dipping.

Approximately 5 km to the east of JDF-6, the Primary fault (Fig. 3*c*, C–C′ (JDF-4)) also exhibits a large step in velocity contours and a termination of some reflectors across the Devil's Mountain fault. The fault, although generally similar to that observed to the west, is broader (Fig. 3*c*). Truncation of the reflections suggests that the dip of the Devil's Mountain fault is again subvertical to moderately north dipping. To the south, the pre-Tertiary basement is at ~1.1 s, similar to section B–B′. The Devil's Mountain fault offsets (north-side-up) the basement by ~0.5 s and the uppermost Pliocene by ~0.4 s (~350 m); both offsets are slightly greater than those to the west. Further to the south of the Primary fault on JDF-4, which transects the deepest part of the basin, the uppermost Pliocene commonly exceeds the depth of the velocity models. The thickness of the Pleistocene rocks is also greater reaching ~0.8 s or ~800 m. The basement high at CMP 22000 (Fig. 3*c*) is associated with an east–southeast-trending pre-Quaternary fault (Johnson et al. 2001) that is subparallel to the Utsalady Point fault (Fig. 2) and crosses Whidbey Island. The fault is not observed to offset the pre-Tertiary basement on profile SG-1 to the west, but is related to the basement high at CMP 10000 (Fig. 3*f*) and on profile PS-2.

Despite being only ~4 km further east, the Primary fault, as shown by sections D–D′ (PS-2) (Fig. 3*d*) and E–E′ (SG-1) (Fig. 3*e*), is located ~1.5 km to the south. Akin to lines to the west, the pre-Tertiary basement is again at ~1.1 s to the south of the Devil's Mountain fault and is offset (relative north-up) by ~0.5 s. However, the vertical offset of the uppermost Pliocene is smaller at ~0.2 s from the seismic profile or ~150 m measured from velocity models, indicating less vertical movement on this segment of the Primary fault during the Quaternary. The location of the Devil's Mountain fault is defined by a sharp change in reflection character, with layered sedimentary rocks to the south and opaque basement to the north. The dip of the Devil's Mountain fault at depth is not well constrained, but southerly dips at angles less than ~75° are not consistent with the reflection data.

The Quaternary sediments north–northwest of the Devil's Mountain fault (Fig. 3*d*, CMP 38000–42000), as mapped by Johnson et al. (2000) (Fig. 2), exhibit only minor folding and faulting with some small vertical offsets. For example, ~0.05 s or ~30 m offsets were measured from velocity models for the fault at CMP 40300. Similarly, no large fault offsets are observed ~6 km to the east, where SG-1 (Fig. 3*e*, E–E′) crosses the mapped Quaternary Devil's Mountain fault near CMP 12200. However, 8 km to the east, section F–F′ (JDF-3C) (Fig. 3*f*) shows a small fault offset (relative north-down) that appears to intersect the seabed suggesting recent activity. Near surface reflections are only offset by 0.05–0.08 s (~40–50 m), but the reflections overlie a larger offset of the pre-Tertiary basement and possibly the uppermost Pliocene of <0.1 s. These offsets are comparable with those (~4–24 m) of the Whidbey formation (age: ~80–130 ka, early Quaternary) on Whidbey Island (Johnson et al. 2001).

The Utsalady Point and Strawberry Point faults

The Utsalady Point fault and Strawberry Point fault were interpreted by Johnson et al. (2001) to be active structures that cut the eastern end of the eastern Juan de Fuca Strait. Reversal in the sense of vertical motion, folding, and the geometry of regional faulting suggest that the Utsalady Point and Strawberry Point faults are left-lateral transpressional faults (Johnson et al. 2001). Approximately 2 m of left-lateral offset has been interpreted as late Holocene from trenches across the Utsalady Point fault (Johnson et al. 2003). Near Whidbey Island, the Utsalady Point fault shows the largest vertical offsets (relative north-up) and forms the southern margin of a pre-Tertiary basement horst (Johnson et al. 2001). Between the two faults, Upper Pleistocene strata show considerable deformation with dips as high as 45° (Johnson et al. 2001).

The Utsalady Point fault on section F–F′ (Fig. 3*f*) has similar reflection, velocity, and structural characteristics to the Primary fault of the Devil's Mountain fault, as interpreted on profiles to the west. Although not clearly imaged, the pre-Tertiary basement may have a vertical offset of ~0.3 s or ~300 m as estimated from the velocity model. The uppermost Pliocene is vertically offset by ~0.05–0.1 s (~40–70 m) with smaller offsets of overlying rocks, indicating Quaternary fault motion. The Strawberry Point fault (SPF) (Fig. 3*f*) is a much smaller feature than the neighbouring Utsalady Point fault, with a south-up sense of throw and a steep dip. The uppermost Pliocene appears to have been vertically offset by ~0.08 s (~70 m), with smaller offsets for the overlying Quaternary rocks.

Faulting associated with the Devil's Mountain fault zone

Mapping by Johnson et al. (2001) suggested that numerous compressional and transpressional features (Fig. 2) represent synthetic deformation (Christie-Blick and Biddle 1985) oblique to the Devil's Mountain fault, which is inferred to be a master fault. The seismic profiles and velocity models presented here provide additional information on some of the previously mapped structures and identify a number of new faults.

South of the Primary fault on section G–G′ (SG-1) (Fig. 4*a*) velocity models reveal a velocity high with several radiating near-linear velocity anomalies that appear to converge at a depth of ~700 m. These anomalies correspond to broken reflections on seismic profiles that show variable senses of offset. The faults may represent a positive flower structure

related to Quaternary strike-slip motion in the Devil's Mountain fault zone.

Several other faults and folds on profile SG-1 have a style and orientation that can be interpreted as having resulted from deformation within a strike-slip system (Christie-Blick and Biddle 1985). A decrease in the magnitude and vertical gradient of velocity to the south of CMP 4500 (SG-1) (Fig. 4*b*) corresponds to a zone of pre-Quaternary faults (Johnson et al. 2000), which we re-interpret to dip north. To the south of the Devil's Mountain fault (CMP 12500-16000), numerous folds in the uppermost Pliocene may be associated with faulting (Fig. 3*e*).

Two faults (Fig 3*b*, CMP 27000-28000) with a steep northward dip and offsets of ~0.02 s (~20–40 m) are observed in Haro Strait. The faults cut the very shallow surface, implying recent motion, and may indicate that some of the motion on the Devil's Mountain fault is taken up by deformation in Haro Strait, as suggested by Johnson et al. (2001).

Discussion

By locating offsets in the Tertiary and Quaternary stratigraphy, the tomographic velocity models and seismic reflection profiles have significantly aided in the interpretation of faults in the eastern Juan de Fuca Strait. Seismic reflection profiles suggest that primary Tertiary motion on the Devil's Mountain fault (Fig. 3; A–A′, B–B′, C–C′) was accommodated to the east of 122.95°W on the Primary fault. This fault divides shallow, high-velocity basement to the north from thick sedimentary deposits to the south, and thus was a northern boundary of the Tertiary Everett basin. The dip of the Primary fault is not precisely constrained by our seismic images or velocity models; however, the steep truncation of seismic reflections from sediments to the south of the fault (Fig. 3) limits any south-dipping fault to be subvertical. To the north of the Devil's Mountain fault, near-surface truncated or broken reflections constrain the dip to a fairly high angle, but the direction is unclear. Deeper reflections on the north side of the fault are rarely present, implying that a wide range of northerly dips is consistent with the seismic reflection data. If the north-dipping reflections at 1.0–1.5 s between CDP 3000 and CDP 5000 on section A–A′ are from the fault, and are not side-scattered noise, then a dip of ~30° is implied at this location. Although the dip of the Devil's Mountain fault is not precisely constrained by our data, we infer a moderate to steep northerly dip, which is similar to the steep northerly dip interpreted for the Devil's Mountain fault on Whidbey Island (Oldow 2000) and the northerly dips inferred for the Leech River and Survey Mountain faults at the southeast tip of Vancouver Island. Reverse motion on the Devil's Mountain fault is also consistent with the compression that commenced in the Late Eocene (Johnson et al. 1996), giving rise to the folding mapped to the north of the fault by previous workers and in this study (Fig. 3*a*).

Based on the similar geometry and the large magnitude of pre-Tertiary basement offset of the Primary fault of the Devil's Mountain fault and the Utsalady Point fault to the west of Whidbey Island, we interpret the Primary fault to extend to and include the Utsalady Point fault. This agrees with the results of Oldow (2000) who interpreted the North Whidbey Island fault (coincident with the later-interpreted (Johnson et al. 2001) segments of the Utsalady Point fault and Strawberry Point fault) to be a reverse fault strand associated with the Devil's Mountain fault zone. The Utsalady Point fault follows a subtle bathymetric low (Fig. 5) that is coincident with the south side of a fairly steep magnetic low. The bathymetric low divides an area of roughly flat bathymetry of generally higher elevation to the north from the steep northern slope of the Smith Island Bank to the south (Fig. 5). The lack of identification of deep faulting by Johnson et al. (2001) between PS-2 and JDF-3C, in association with the Utsalady Point fault, is not surprising, based on the sparse deeper seismic coverage at this particular location. Industry line 2 (Johnson et al. 2001), which crosses the Devil's Mountain fault at 122.92°W, shows a change from continuous to discontinuous reflections of the lower Tertiary sedimentary rocks. This change in reflection character is coincident with the trace of the Utsalady Point fault and is likely related to faulting.

Observations of the changing style of the Primary fault may aid in understanding its Tertiary to Quaternary history. Profiles JDF-5, JDF-6, JDF-4, PS-2, and SG-1 (Fig. 3) show a similar thickness of Tertiary rocks in the hanging wall of the Primary fault, suggesting consistent vertical motion during the Tertiary. Section F–F′ (Fig. 3*f*) shows a thinner deposit of Tertiary rocks near to the Primary fault (Utsalady Point fault); however, south of CMP 11000 the Tertiary section reaches a similar thickness to that observed on profiles to the west. An east–southeast-trending pre-Quaternary reverse fault (Johnson et al. 2001) exists subparallel to the Utsalady Point fault ~5 km to the south (Figs. 2, 3*f*). The fault marks the southern limit of a basement high cored by pre-Tertiary rocks (Fig. 3, F–F′, CMP 10000). The basement high associated with this fault is also observed at CMP 22000 on section C–C′ (JDF-4) (Fig. 3*c*,). These observations suggest that Tertiary motion was foremost on the Primary fault, but that east of ~122.95°W, a component of northward Tertiary compression (Johnson et al. 1996) was distributed amongst other structures, including the reverse fault ~5 km to the south. This motion may have included displacement across the Devil's Mountain fault, but our seismic images do not allow estimation of Tertiary offset.

Quaternary left-lateral transpression (Johnson et al. 2000, 2001) resulted in en-echelon faults and folds with a northwest strike, in a zone over 10 km wide along the east-trending Devil's Mountain fault zone. However the intensity and distribution of these structures suggests that deformation was influenced by the older structures. The east–west-trending Primary fault to the west of ~122.95°W formed a segment of the Quaternary Devil's Mountain fault, which is inferred to be a master fault (Johnson et al. 2001).

The uppermost Pliocene to the west of ~122.95°W on sections A–A′, B–B′, and C–′C (Fig. 3) shows a large offset across the Primary fault, suggesting substantial reverse-slip motion during the Quaternary. However, the offset of the uppermost Pliocene across the Primary fault is far smaller on all sections to the east of ~122.95°W (PS-2, SG-1, JDF-3C; Fig 3). High-resolution US Geological Survey line 164 (Johnson et al. 2001) shows the Utsalady Point fault to disrupt the uppermost Pliocene, but not Quaternary, deposits. This observation is in contrast to the Utsalady Point fault on JDF-3C (Fig. 3*f*), ~1 km to the east, where the uppermost

Fig. 5. Structural interpretation of the Devil's Mountain fault zone, modified from the structural interpretation of Johnson et al. (2000). Heavy black solid and dashed lines, trace of the Tertiary Primary fault; heavy grey dashed lines, inferred transfer zones between the Primary fault of the Devil's Mountain fault and Utsalady Point fault. DMF, Devil's Mountain fault; SWFZ, Southern Whidbey Island fault zone.

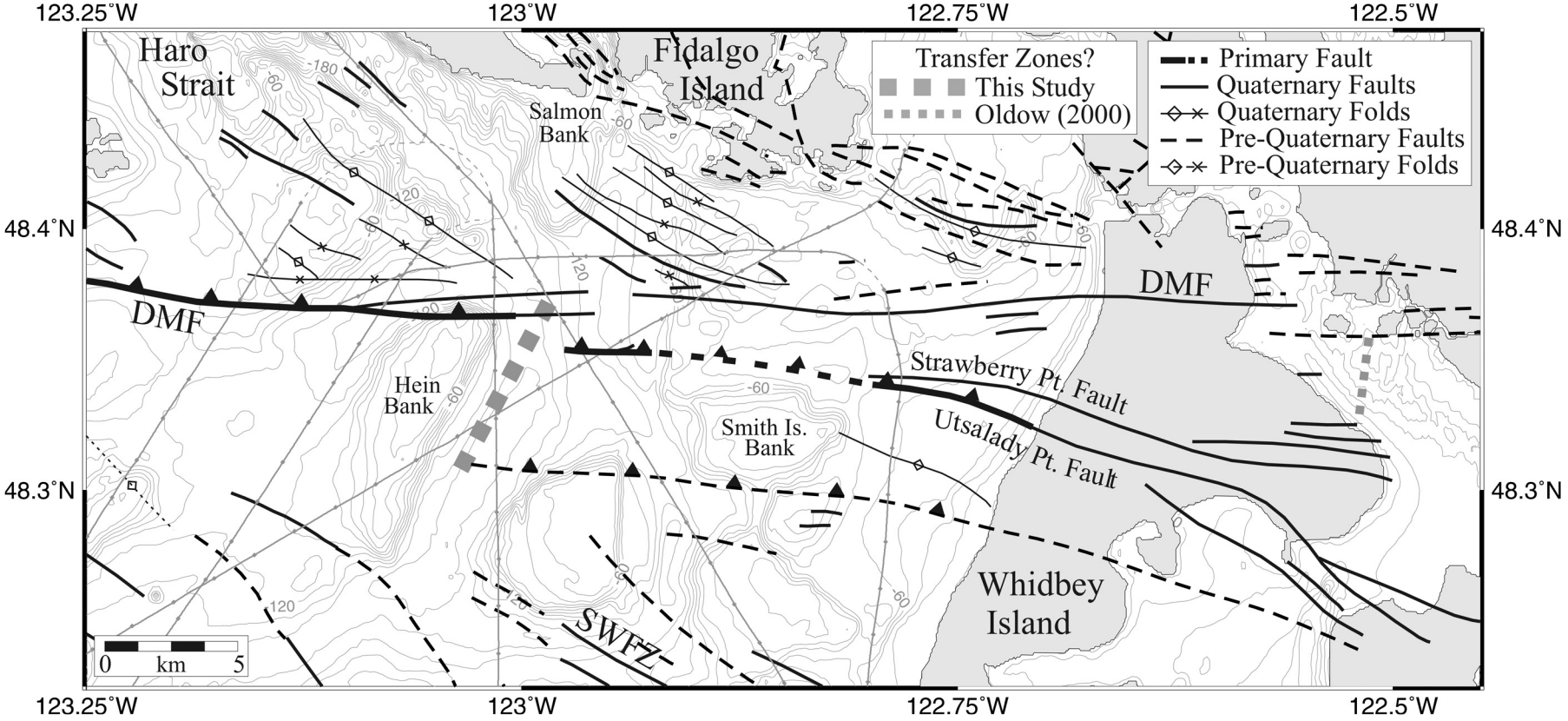

Pliocene is vertically offset by ~0.05–0.1 s (~40–70 m). This offset is lower than the interpretation of 200–300 m by Johnson et al. (2001), which was inferred from seismic reflection profiles and well data on Whidbey Island, and likely indicates that the amount of vertical offset varies along strike. The Strawberry Point fault also appears to exhibit along-strike offset variation of the uppermost Pliocene with ~0.08 s (~70 m) for JDF-3C (Fig. 3*c*) compared with an estimate of 80–200 m uplift of the uppermost Pliocene on the west side of Whidbey Island (Johnson et al. 2001). Seismic profiles suggest that there is no offset of Quaternary strata on the Utsalady Point fault west of ~122.8°W and east of ~122.9°W. Variations in the amount of offset of Quaternary strata across the Utsalady Point fault, as documented by Johnson et al. (2001) and by this study, may indicate that motion has been distributed to nearby faults. Transpression responsible for uppermost Pliocene uplift along the Primary fault east of ~122.95°W may have been distributed to northwest-striking compressional structures to the southeast of Salmon Bank. Similar northwest-striking structures are observed on profile JDF-3B to the southwest of Salmon Bank and in Haro Strait. However, faulting here shows less intensity, with smaller fault offsets.

To the east of Whidbey Island, Oldow (2000) suggested that a north–northeast-trending oblique ramp system links the eastern end of the North Whidbey Island fault (coincident with the Strawberry Point fault of Johnson et al. (2001)) to the Devil's Mountain fault just west of the Skagit delta. A similar oblique ramp, of Tertiary age, might explain the ~1.5 km offset of the Primary fault at ~122.95°W and the change in style of the Devil's Mountain fault zone from a single reverse fault to a number of such faults. This interpretation is similar to the high-angle tear faults between thrust sheets along the Seattle fault (Johnson et al. 1999; Brocher et al. 2004). Several observations support the interpretation of a change in structural style and a possible NNE-trending Tertiary transfer system:

(1) The reduction in uppermost Pliocene offset on the Primary fault to the east of ~122.95°W suggests that Quaternary deformation may have been focused on the Primary fault to the west, but distributed amongst other structures to the east.
(2) Quaternary oblique faults and folds (Johnson et al. 2001) in Haro Strait and adjacent to Salmon Bank (Fig. 5) are more common and the faults show greater offsets to the east of ~122.95°W, suggesting that Tertiary structures may be influencing their development.
(3) The coincident western termination of the pre-Quaternary reverse fault that strikes subparallel ~5 km to the south of the Utsalady Point fault.
(4) The linearity of the southeastern flank of Hein Bank is suggestive of structural control, and is coincident with a boundary between Holocene – Post-glacial stratified and unstratified glacial marine surficial sediments (Hewitt and Mosher 2001).
(5) Magnetic anomalies (Blakely and Lowe 2000) to the south of the Devil's Mountain fault change from high-amplitudes (~500 nT), which are associated with the highly magnetic Crescent basement (with a magnetic low of ~–200 nT) directly to the south of the Devil's Mountain fault in the west, to a broad region of lower amplitudes (~100 nT), reflecting a change in basement composition and (or) structure to the east.

The ambiguity in the estimated dip of the Primary fault of the Devil's Mountain fault zone makes it difficult to discriminate clearly among different evolutionary models. If the dip of the fault at depth is relatively low, then it may have developed as part of a passive roof duplex, as suggested by Oldow (2000), with the fault merging into a deeper roof thrust, as has been proposed for a number of faults mapped in the Seattle uplift of the Puget Lowlands (Brocher et al. 2004). The Devil's Mountain fault zone may then have localized strain under changing kinematic conditions, resulting in the left-lateral slip that has been inferred on the fault in more recent times. If, however, the Primary fault has a steep northerly, or even a near-vertical southerly dip, which is permitted by the seismic reflection data, then the fault is likely part of a transpressive fault system that is inconsistent with the suggested passive roof duplex model. If the Tertiary sedimentary stratigraphy could be traced continuously beneath the surface location of the Devil's Mountain fault, then a shallower dip for the fault would be confirmed. This cannot be accomplished with the existing reflection data, which were acquired for crustal-scale imaging. However, seismic data acquired with a finer spatial sampling would provide the necessary high fold at travel times of around 1.0 s to permit imaging of sedimentary reflectors beneath an overburden with laterally varying velocity, especially if constraints on the velocity model from long-offset first arrivals were also available.

Conclusions

(1) The Tertiary Primary fault of the Devil's Mountain fault zone to the west of ~122.95°W and the large offset fault (Utsalady Point fault) to the southeast on profiles SG-1 and PS-2 have a similar character that suggests that they are of the same origin. We conclude that the Tertiary Primary fault of the Devil's Mountain fault zone is an extension of the Utsalady Point fault. These faults show the largest Tertiary offsets in the Devil's Mountain fault zone and form the approximate northern boundary of the Tertiary Everett basin.
(2) The Devil's Mountain fault originally developed as a north-dipping reverse fault during Tertiary north–south compression. However, during the evolution of the Everett Basin, the western segment of Primary fault of the Devil's Mountain fault zone likely separated from the what is now the Utsalady Point fault, along a Tertiary aged oblique trending transfer fault, resulting in the ~5 km offset that exists today.
(3) Quaternary left-lateral transpressive motion was influenced by a number of Tertiary structures, but was focussed on the Devil's Mountain fault. Quaternary offsets on the Primary fault east of ~122.95°W are smaller than those to the west. This suggests that a component of northward compression was accommodated on the Utsalady Point fault and oblique compressional structures, which are most prevalent to the north of the Devil's Mountain fault to the east of ~122.95°W. Evidence for Quaternary deformation is not observed on the reverse fault to the south of the Utsalady Point fault.

(4) Holocene deformation has focussed on the Devil's Mountain fault, and the Utsalady Point and Strawberry Point faults to the east of ~122.8°, indicating that these are active structures. Holocene deformation has not affected the Utsalady Point fault to the west of ~122.8°W, but there appears to be a high potential for reactivation.

Acknowledgments

We thank Dr. Jonathan C. Lewis and Dr. Dan Gibson for discussions of fault structure and geometry. Constructive comments from Tom Brocher, Stephen Johnston, John Oldow, Dave Mosher, and an anonymous reviewer helped to improve the final version of the paper. This project was funded by the National Earthquake Hazards Program of the US Geological Survey under Grant 02HQGR0055 and the Natural Sciences and Engineering Research Council of Canada.

References

Aldridge, D.F., and Oldenburg, D.W. 1993. Two dimensional tomographic inversion with finite difference traveltimes. Journal of Seismic Exploration, **2**: 257–274.

Atwater, B., and Moore, A.L. 1992. A tsunami about 1000 years ago in Puget Sound. Science, **258**: 1614–1616.

Blakely, R., and Lowe, C. 2000. Aeromagnetic anomalies of the eastern Juan de Fuca Strait region. *In* Neotectonics of the eastern Juan de Fuca Strait; a digital geological and geophysical atlas. *Edited by* D.C. Mosher and S.Y. Johnson. Geological Survey of Canada, Open File Report 3931.

Booth, D.B. 1994. Glaciofluvial infilling and scour of the Puget Lowland, Washington, during ice-sheet glaciation. Geology, **22**: 695–698.

Brocher, T.M., Parsons, T., Blakely, R.J., Christensen, N.I., Fisher, M.A., Wells, R.E. et al. 2001. Upper crustal structure in Puget Lowland, Washington: results from the 1998 Seismic Hazards Investigation in Puget Sound. Journal of Geophysical Research, **106**(B7): 13 541 – 13 564.

Brocher, T.M., Blakely, R.J., and Wells, R.E. 2004. Interpretation of the Seattle Uplift, Washington, as a passive-roof duplex. Bulletin of the Seismological Society of America, **94**(4): 1379–1401.

Calvert, A.J., Fisher, M.A., Johnson, S.Y., and the SHIPS Working Group. 2003. Along-strike variations in the shallow seismic velocity structure of the Seattle fault zone: evidence for fault segmentation beneath Puget Sound. Journal of Geophysical Research, **108**(B1): 2005. doi:10.1029/2001JB001703.

Christie-Blick, N., and Biddle, K.T. 1985. Deformation and basin formation along strike-slip faults. *In* Strike-slip deformation, basin formation, and sedimentation. *Edited by* K.T. Biddle, and N. Christie-Blick. Society of Economic Paleontologists and Mineralogists, Special Publication 37, pp. 1–34.

Clowes, R.M., Brandon, M.T., Green, A.G., Yorath, C.J., Sutherland Brown, A., Kanesewich, E.R. et al. 1987. LITHOPROBE — southern Vancouver Island: Cenozoic subduction complex imaged by deep seismic reflection data. Canadian Journal of Earth Sciences, **24**: 31–51.

Dragert, H., Hyndman, R.D., Rogers, G.C., and Wang, K. 1994. Current deformation and the width of the seismogenic zone of the northern Cascadia subduction thrust. Journal of Geophysical Research, **99**: 653–668.

Fisher, M.A., Brocher, T.M., Hyndman, R.D., Tréhu, A.M., Weaver, C.S., Crosson, R.S. et al. 1999. Seismic survey probes urban earthquake hazards in Pacific northwest. EOS Transactions of the American Geophysical Union, **80**(2): 16–17.

Gower, H.D., Yount, J.C., and Crossen, R.S. 1985. Seismotectonic map of the Puget Sound region, Washington. US Geological Survey. Miscellaneous Investigations Series, Map I-1613, scale 1 : 250 000.

Hewitt, A.T., and Mosher, D.C. 2001. Late Quaternary stratigraphy and seafloor geology of eastern Juan de Fuca Strait, British Columbia and Washington. Marine Geology, **177**: 295–316.

Hyndman, R.D., Yorath, C.J., Clowes, R.M., and Davis, E.E. 1990. The northern Cascadia subduction zone at Vancouver Island: seismic structure and tectonic history. Canadian Journal of Earth Sciences, **27**: 313–329.

Hyndman, R.D., Mazzotti, S., Weichert, D.H., and Rogers, G.C. 2003. Frequency of large crustal earthquakes in Puget Sound – southern Georgia Strait predicted from geodetic and geological deformation rates. Journal of Geophysical Research, **108**(B1): 1–12.

Johnson, S.Y. 1985. Eocene strike-slip faulting and nonmarine basin formation in Washington. *In* Strike-slip deformation, basin formation, and sedimentation. *Edited by* K.T. Biddle and N. Christie-Blick. Society of Economic Paleontologists and Mineralogists, Special Publication 37. pp. 283–301.

Johnson, S.Y., Potter, C.J., Armentrout, J.M., Miller, J.J., Finn, C., and Weaver, C.S. 1996. The southern Whidbey Island fault, an active structure in the Puget Lowland, Washington. Geological Society of America Bulletin, **108**: 334–354.

Johnson, S.Y., Dadisman, S.V., Childs, J.R., and Stanley, W.D. 1999. Active tectonics of the Seattle fault and central Puget Sound, Washington – implications for earthquake hazards. Geological Society of America Bulletin, **111**(7): 1042–1053.

Johnson, S.Y., Mosher, D.C., Dadisman, S.V., Childs, J.R., and Rhea, S.B. 2000. Tertiary and Quaternary structures of the eastern Juan de Fuca Strait: interpreted map. *In* Neotectonics of the eastern Juan de Fuca Strait: a digital geological and geophysical atlas. *Edited by* D.C. Mosher, and S.Y. Johnson. Geological Survey of Canada, Open File report 3931.

Johnson, S.Y., Dadisman, S.V., and Mosher, D.C. 2001. Active tectonics of the Devil's Mountain fault and related structures, northern Puget Lowland and eastern Strait of Juan de Fuca region, Pacific Northwest. US Geological Survey, Professional paper 1643.

Johnson, S.Y., Nelson, A.R., Personius, S.F., Wells, R.E., Kelsey, H.M., Sherrod, B.L. et al. 2003. Evidence for one or two late Holocene earthquakes on the Utsalady Point fault, Northern Puget lowland, Washington. Geological Society of America Meeting, Seattle, Wash., Nov. 2–5, 2003.

Lewis, J.C., Unruh, J.R., and Twiss, R.J. 2003. Seismogenic strain and motion of the Oregon coast block. Geology, **31**(2): 183–186.

MacLeod, N.S., Tiffen, D.L., Snavely, P.D., Jr., and Currie, R.G. 1977. Geological interpretation of magnetic and gravity anomalies in the Strait of Juan de Fuca, US–Canada. Canadian Journal of Earth Sciences, **14**: 223–238.

Mazzotti, S., Dragert, H., Hyndman, R.D., Miller, M.M., and Henton, J.A. 2002. GPS deformation in a region of high crustal seismicity: N. Cascadia forearc. Earth and Planetary Sciences Letters, **198**: 41–48.

McCaffrey, R., Johnson, C.K., Zwick, P.C., Long, M.D., Goldfinger, C., Nabalek, J.L. et al. 2000. Rotation and plate locking along the southern Cascadia subduction zone. Geophysical Research Letters, **21**: 3117–3120.

Mosher, D.C., and Hewitt, A.T. 2004. Late Quaternary deglaciation and sea-level history of eastern Juan de Fuca Strait, Cascadia. Quaternary International, **121**: 23–29.

Mosher, D.C., and Johnson, S.Y. 2000. Neotectonics of the eastern Juan de Fuca Strait: a digital geological and geophysical atlas. Geological Survey of Canada, Open File report 3931.

Muller, J.E. 1983. Geology, Victoria. Geological Survey of Canada, Map 1553A, scale 1 : 100 000.

Nedimović, M.R., Mazzotti, S., and Hyndman, R.D. 2003. Three-dimensional structure from feathered two-dimensional seismic reflection data; the eastern Nankai trough. Journal of Geophysical Research, 108(B10): 2456. doi:10.1029/2002JB001959: 1–14.

Oldow, J.S. 2000. Fault characterisation and assessment of slip on the Devil's Mountain and North Whidbey Island fault systems, northwestern Washington. USGS Technical Report 276.

Rusmore, M.E., and Cowan D.S. 1985. Jurassic–Cretaceous rock units along the southern edge of the Wrangellia terrane on Vancouver Island. Canadian Journal of Earth Sciences, **22**: 1223–1232.

Tabor, R.W. 1994. Late Mesozoic and possible early Tertiary accretion in western Washington state — the Helena–Haystack melange and the Darrington – Devil's Mountain fault zone. Geological Society of America Bulletin, **106**: 217–232.

Weaver, C.S., and Smith, S.W. 1983. Regional tectonic and earthquake hazard implications of a crustal fault zone in southwestern Washington. Journal of Geophysical Research, 88(B12): 10 371 – 10 383.

Wells, R.E., Weaver, C.S., and Blakely, R.J. 1998. Forearc migration in Cascadia and its neotectonic significance. Geology, **26**: 759–762.